Science of the Total Environment 908 (2024) 168378

Contents lists available at ScienceDirect

Science of the Total Environment

journal homepage: www.elsevier.com/locate/scitotenv

Microplastics attenuation from surface water to drinking water: Impact of treatment and managed aquifer recharge – and identification uncertainties

Daniele la Cecilia [a,*,1], Matthias Philipp [b], Ralf Kaegi [b], Mario Schirmer [a,c,d], Christian Moeck [a]

[a] Department Water Resources and Drinking Water, Swiss Federal Institute of Aquatic Science and Technology Eawag, Dübendorf, Switzerland
[b] Department of Process Engineering, Swiss Federal Institute of Aquatic Science and Technology Eawag, Dübendorf, Switzerland
[c] Centre of Hydrogeology and Geothermics (CHYN), University of Neuchâtel, Neuchâtel, Switzerland
[d] Department of Geology and Geological Engineering, Laval University, Quebec, Canada

HIGHLIGHTS

- Rhine River bed water MPs mean concentration equalled 112 ± 27.4 MPs/l.
- Secondary treatment MPs removal efficiency achieved 98.6 %.
- Fragments prevailed over fibers everywhere but fibers were longer and more in river water.
- We observed great heterogeneity in the distribution of surrogate MPs on the filter.
- Classification uncertainty do not affect the decreasing trend of MPs concentrations.

GRAPHICAL ABSTRACT

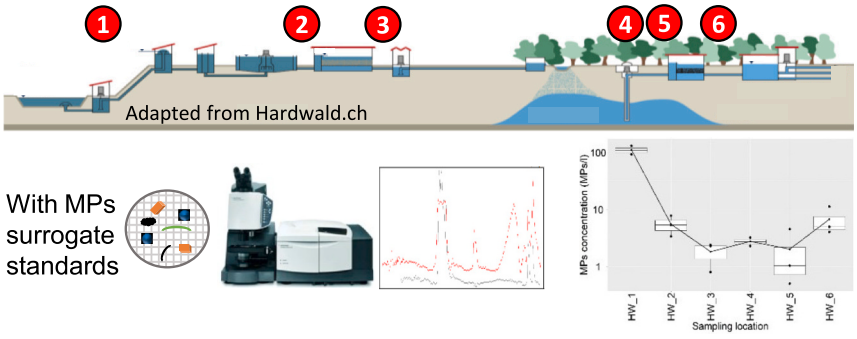

ARTICLE INFO

Editor: Damiá Barceló

Keywords:
Microplastics
Groundwater
Managed aquifer recharge
Drinking water
Water treatment

ABSTRACT

River water can be used to recharge aquifers exploited for drinking water production. Several recent studies reported microplastics (MPs) in river water, and therefore, the potential contamination of groundwater by MPs is a growing concern among stakeholders and citizens. In this research, we investigate the fate of MPs (> 20 μm) along six different stages of a major Managed Aquifer Recharge (MAR)-water supply system in Switzerland. About 20 l of water were filtered using steel meshes at each location in triplicates. In the laboratory, MPs deposited on the anodisc filters were identified using Focal Plane Array (FPA) micro-Fourier-Transform-InfraRed (μFTIR) spectroscopy. The obtained hyperspectral data were processed using the imaging software Microplastics Finder for MPs identification and classification. Our results revealed a 20-fold decrease in MPs concentration from the Rhine River bed water (112 ± 27.4 MPs/l) to after the coagulation, flocculation and sedimentation (5.5 ± 2.2 MPs/l), a further 3-fold decrease to after the sand-filtration system (1.8 ± 0.9 MPs/l), corresponding to an overall removal efficiency of 98.4 %. The MPs concentrations remained low following MAR (2.7 ± 0.7 MPs/l) through a Quaternary gravel aquifer. Activated carbon filters did not substantially further reduce MPs concentrations. The percentage of fragments (≈95 %) prevailed over fibers (≈5 %) at all locations, with fibers being longer and more abundant in the river water. Overall, this study demonstrates the effectiveness of the treatment systems to remove MPs larger than 20 μm. Finally, we calculated an uncertainty in MPs concentrations of one

* Corresponding author at: Department Water Resources and Drinking Water, Eawag, 8600, Dübendorf, Switzerland.
E-mail address: daniele.lacecilia@eawag.ch (D. la Cecilia).
[1] Now at Department of Civil, Environmental and Architectural Engineering, University of Padova, Padova, Italy.

https://doi.org/10.1016/j.scitotenv.2023.168378
Received 4 September 2023; Received in revised form 1 November 2023; Accepted 4 November 2023
Available online 10 November 2023

order of magnitude depending on the user-defined parameters inside the MPs identification and classification model. The Quality Assurance/Quality Control approach followed during laboratory analysis highlighted an accumulation of surrogate particles at the edges of the disc, which would have an impact for MPs number upscaling.

1. Introduction

With the production of plastics reaching almost 400 million tons globally in 2021 (exclusively including thermoplastics and thermosets) (PlasticEurope, 2022) and its ubiquitous occurrence in the environment (Tian et al., 2023), we have entered the *Plasticene* era (Reed, 2015). While there is still no consensus on the definition of microplastics (MPs) (Frias and Nash, 2019), the majority of studies reviewed by Hartmann et al. (2019) defined MPs as particles with a size ranging between 1 μm and 5 mm, as previously suggested in Arthur et al. (2009). Primary MPs are intentionally produced for textiles manufacturing, cosmetics and personal care products production and industrial processing. Secondary MPs occur following weathering and fragmentation of larger plastic items (Hale et al., 2020). Primary and secondary MPs enter aerial, aquatic and terrestrial ecosystems through a wide range of sources and transport processes (Waldschläger et al., 2020).

Sources of MPs in surface water including wet and dry atmospheric deposition (Kernchen et al., 2022), runoff from urban (Ross et al., 2023; Treilles et al., 2021) and agricultural lands (Crossman et al., 2020) as well as effluents from wastewater treatment plants (Xu et al., 2023) may hinder the use of surface water to address water availability challenges. Groundwater is increasingly being exploited globally (Wada, 2016), and yet, even groundwater is subject to MPs contamination (Belkhiri et al., 2022; Moses et al., 2023; Re, 2019). Goeppert and Goldscheider (2021) and Panno et al. (2019) show that transport of MPs in alluvial and karst aquifers over larger distances is possible, but quantitative studies regarding the direct input of MP through groundwater management practices such as managed aquifer recharge (MAR) are still lacking.

Reports on the occurrence of MPs in drinking water urged scientists to assess the capability of drinking water treatment plants to remove MPs from water sources and to identify the sources of MPs in drinking water (Johnson et al., 2020; Koelmans et al., 2019; Mintenig et al., 2019; Pivokonsky et al., 2018; Schymanski et al., 2021; Strand et al., 2018). An assessment of the MP retention may be particularly important at MAR sites (Re, 2019; Viaroli et al., 2022) or at locations where water abstraction is near rivers with groundwater-surface water interaction (Boos et al., 2021). Rivers and streams act as a transport vector for MPs. Drinking water production plants were not designed for MPs removal, but they do sequester particles in the water source by a sequence of processes including flocculation, sedimentation and filtering (Acarer, 2023). The level of treatment depends on the quality of the water source, which is affected by the anthropization of the catchment, and is essential in order to provide the society with safe drinking water (Rosario-Ortiz et al., 2016; Velasco et al., 2023).

Studies have shown that the sequence of processes in drinking water production plants typically retain >85 % of incoming MPs particles (Johnson et al., 2020; Mintenig et al., 2019; Pivokonsky et al., 2018; Wang et al., 2020). Nonetheless, the most effective treatment train to remove MPs from influent water is still under debate (Pivokonsky et al., 2018). Coagulation, flocculation and sedimentation processes altogether could remove 50 % of MPs (Wang et al., 2020) up to 62 % of MPs (Pivokonsky et al., 2018). The following treatment by means of sand filtration reduced MPs by an additional ≈10 % (Wang et al., 2020). Sand filtration alone could remove up to 70 % of MPs in a non-polluted catchment (Pivokonsky et al., 2018). In two highly polluted catchments, the earlier use of flotation technology removed 81 % of MPs, whereas resorting to sedimentation instead resulted in the removal of 82 % of MPs (Pivokonsky et al., 2018). Therefore, the physical and chemical processes affecting the fate of MPs must be understood in order to design effective water treatment processes for MPs removal but can be very site specific. Two studies clearly revealed the processes affecting the efficiency removal of sand filtration system by monitoring nanoplastics. In particular, Ramirez Arenas et al. (2022) shows that sand filtration removes 99.2 % of polystyrene nanoplastics in the presence of coagulant, as compared to a much lower 54.3 % without coagulant. Pulido-Reyes et al. (2022) finds that the formation of a biofilm on the sand filtration media was key for achieving a 99 % removal of palladium-labelled nanoplastics.

In this study, we quantify the sequestration of MPs larger than 20 μm from surface water to drinking water in a major MAR-drinking water supply system in Switzerland. The system is designed to capture the Rhine River water from the river bed, it undergoes secondary treatment (coagulation with iron chloride, $FeCl_3$, when the turbidity is high – at very high turbidity, river water intake is stopped –, flocculation and sedimentation and sand filtration), MAR into a sand-gravel aquifer and tertiary treatment (activated carbon filter and UV disinfection) after groundwater abstraction. We address the capability of the pre-treatment to protect groundwater during MAR through an adequate removal of MPs and investigate MPs fate along the system. Finally, we investigate the role of user defined model parameters for MPs identification and classification on the output MPs concentrations as well as how using MPs surrogate standard can clearly reveal the particles spatial distribution on the filter to analyze, which would have an impact for MPs number upscaling.

2. Methods

2.1. Study area

The study area is located in north-western Switzerland (Fig. 1) and is an essential drinking water production site for the region. At this study site, Rhine river bed water is artificially infiltrated for groundwater recharge through channels and ponds and subsequently used for drinking water production. Annually, about 33 million m^3 of Rhine river bed water are artificially infiltrated, whereas about 14.2 million m^3 of groundwater are extracted. Due to the high infiltration rates, a hydraulic barrier is created in the recharge area, which protects the groundwater from the urban and industrial influences present in the vicinity of the drinking water extraction area. Several field and modeling studies have been conducted to better quantify the impact of artificial infiltration, MAR recharge efficiency and transport of materials from urban and industrial areas (Moeck et al., 2017a,b; Popp et al., 2019).

The Rhine water is intercepted from the river bed using a covered outlet. The water flows through the pipe into the pump station. The pump station represented the first sampling location (HW_1, where HW is the abbreviation of the water company name and the number refers to the sequential order of the sampling locations along the MAR-water supply system).

From this location, the Rhine river bed water is pumped 20 m up into the overflow station. Then, the water undergoes coagulation ($FeCl_3$) and flocculation in a sedimentation tank. The coagulation only happens in the seldom case of high turbidity but the river water intake is not yet stopped. It is possible to sample the treated water, still considered raw by the company, directly from a pipe that terminates with two taps. One tap is an official sampling point used for routine chemical analysis for regulatory controls (Moeck et al., 2016) and it is considered as our second location (HW_2). The outflow is passed through a sand-filter to remove fine particles that did not settle in the pre-treatment. The filtered

water represents location HW_3.

The water is then pumped to the eastern side of the nearby forest for managed aquifer recharge. The detailed geological and hydrogeological description of the study area refers to previous studies (Moeck et al., 2017a; Epting et al., 2022). In brief, water is distributed within the 3500 m long infiltration channels (total recharge area: 7000 m^2) and in the six ponds (total recharge area: 4000 m^2). The distribution of the surface water follows the flow gradient (east to west) and uses manually adjusted weirs that also regulate the distribution between the parallel channels. The bottom of the infiltration channels and ponds contain an approximately 50 cm thick artificial gravel layer (gravel size around 0.5 to 1.0 cm), on top of the natural soil with natural gravels, to facilitate infiltration into the subsurface. The amount of surface water inducted into the infiltration system is adjusted to the expected water demand, which is associated with changing extraction rates at the drinking water wells. Infiltration occurs into a Quaternary Rhine gravel aquifer. The fluvial–glacial gravels from Quaternary strata have a varying thickness of 5–50 m on top of the bedrock. The thickness close to the main drinking water wells is around 20–40 m. The unsaturated zone between the artificial infiltration system and the pumping wells can vary between 18 and 35 m, depending on the pumping and infiltration rates and the location. The average hydraulic conductivity is 3.1×10^{-3} m/s. The distance between the infiltration system and drinking water wells in the north is roughly 400 m.

Pumped groundwater (HW_4) is delivered for tertiary treatment using an activated carbon filter to remove micropollutants and UV treatment for water disinfection. The sampling location before the activated carbon filter is named HW_5 and the one after is called HW_6. No further water treatment happens between HW_4 and HW_5.

2.2. Sampling material preparation

For the collection of the suspended solids, stainless steel meshes (20 μm mesh size, diameter 47 mm, mesh 500, Zivipf.de) were used. Before sampling, steel filters and glass containers were rinsed first with Milli-Q® water and then with ethanol (70 %, RC-FSP-018, Reuss Chemie). The cap of the glass container was made of an internal layer of rubber.

The steel filter was accommodated inside an metal device (Fig. 2a), which allowed for easily connecting to water taps in industrial plants and for creating closed filter units to avoid filter contamination by MPs from the air. The metal device was used at all locations. The water distribution network along the water supply system has taps used for sampling water for quality analysis. When the direct connection to taps was not possible due to different sizes, we used a silicon tube to adapt our device to the tap and Teflon tape to seal junctions. Before inserting the stainless steel filter, we flushed the connection for 30 s to remove fragments possibly created by abrasion. Any cross-contamination from silicon is summarized in Section 3.2.

Inside the pumping station at HW_1, a metal bucket secured using a coconut fiber-made rope was lowered to the reservoir to collect the incoming raw Rhine River bed water. The water volume was poured through the 123 μm filter inside a steel funnel (pre-washed with Milli-Q® water once) connected to our metal device accommodating the 20 μm steel filter. This pre-filtration was done to retain large particles and prevent the 20 μm mesh to clog after a small sample volume. We used a pump to accelerate the filtration. During filtration, a metal lid covered the funnel to limit cross-contamination from the air.

2.3. Sampling campaign

The sampling campaign happened on June 22nd, 2022 (from HW_2 to HW_6) and on February 22nd, 2023 (HW_1). The Rhine River bed water at HW_1 was sampled at a later stage after the analysis of the samples showed very low MPs abundances already at the initial stages of the MAR system. Visual inspection of the 123 μm steel filter did not reveal large plastic material, which may be explained by the fact the Rhine River water was captured from the riverbed. Therefore, we did not analyze the 123 μm steel filter in further detail.

We filtered 20 l of water in triplicates at most location. Due to clogging of the 20 μm steel filter, 15 l were collected for the second and third replicas at HW_1. On average, filtration lasted at each location about 2 h. This long filtration time was due to the low flow coming from

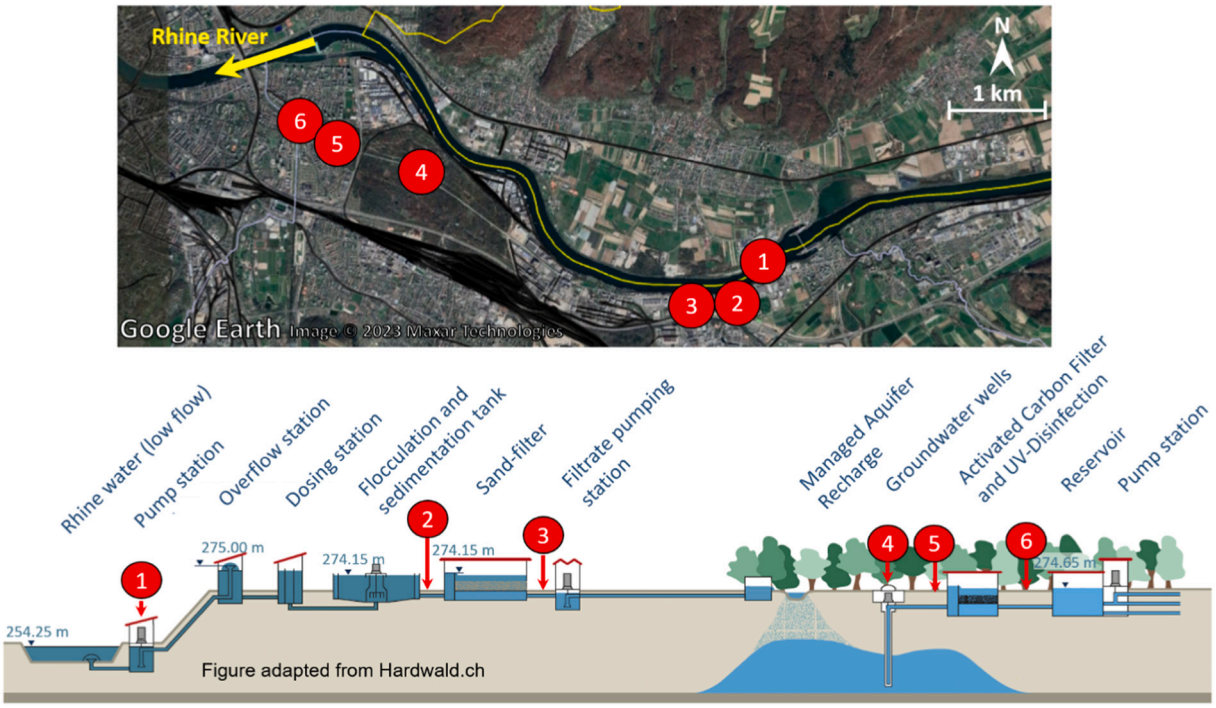

Fig. 1. The top panel shows the study area through a satellite image sourced from Google Earth Pro. The bottom panel pictures the MAR-water supply system modified from hardwasser.ch. Piping connect HW_4 with HW_5 without any further treatment in between.

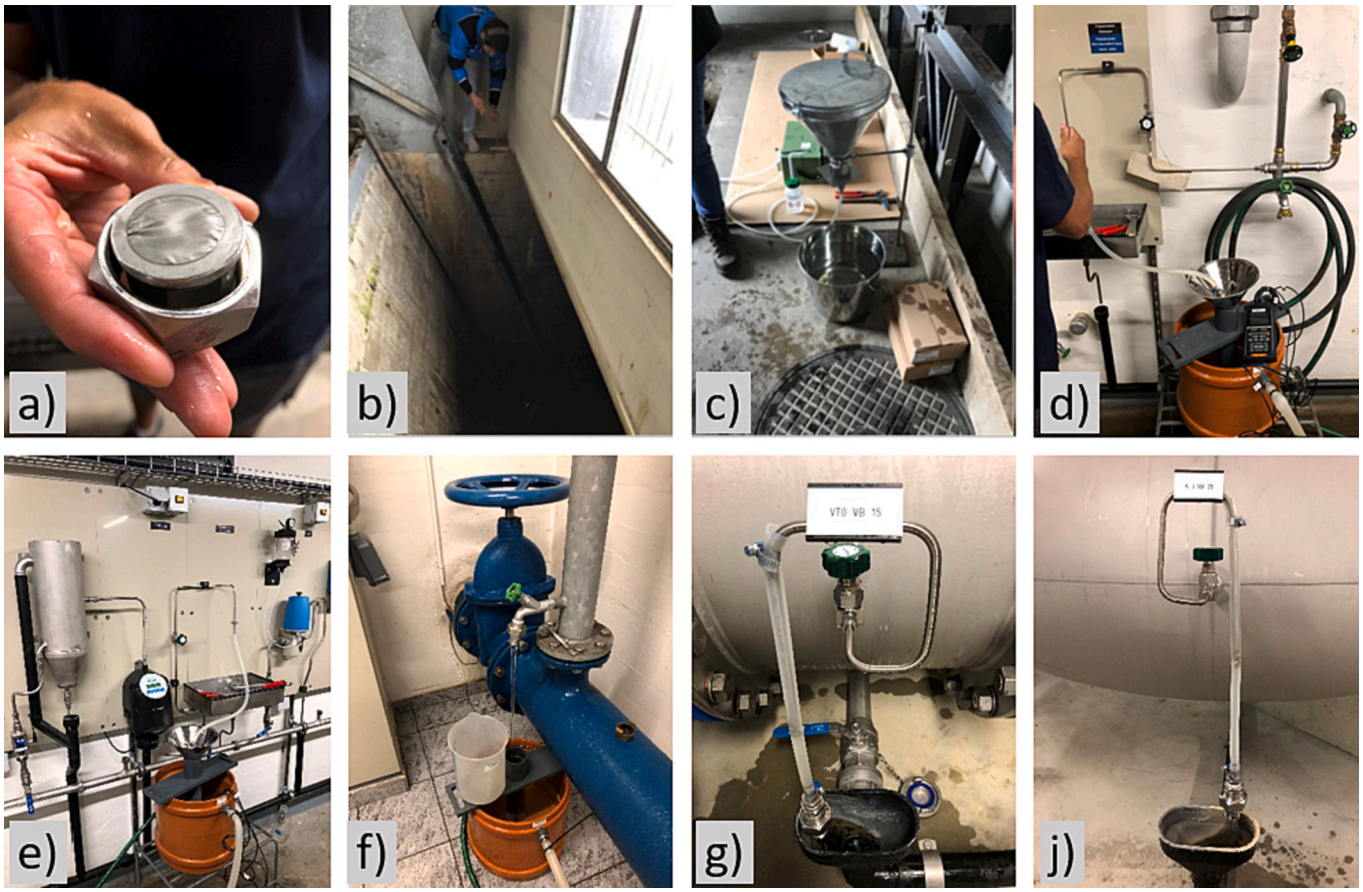

Fig. 2. Photos of: a) stainless steel filter partially inserted within the metal device; b) withdraw of river water at HW_1 using a bucket secured with a rope made of coconut fibers; c) Surface water pumping-aided filtration setup covered with a stainless steel lid; d) Silicon connection to HW_2; e) Silicon connection to HW_3; f) Teflon sealing at HW_4; g) Silicon connection at HW_5; j) Silicon connection at HW_6.

the taps. In fact, the MAR system was designed to let gravity drive the water flow from the overflow station until the pumps before the infiltration channels. Thus, the filtration of higher volumes was not possible due to time constraints. Yet, we preferred to maintain the filtration volume of 20 l also at the locations downstream for comparability of the sampling approach.

We collected one field blank at each location by leaving one clean bottle open during the acquisition of the three replicas, although we did not expect cross contamination from air given that we sampled the water flowing into pipes (results on microplastics counts are presented in Section S1).

The steel filters inside their bottles and the blanks were stored at 4 °C for about one month before sample preparation and analysis.

2.4. Sample preparation and analysis

The steel filters inside their bottles were brought from the cold room to the laboratory (19–21 °C) to warm up for one hour before sample preparation. Blue polyethylene (PE) spheres (53 μm to 63 μm diameter) were used as surrogate standards to estimate the sample specific recoveries as outlined by Philipp et al. (2022). We referred to these particles as blue PE spheres. The blue PE spheres were deposited on a glass slide and imaged using an optical microscope (VHX-7000, Keyence, Japan). We used the image analysis software integrated with the microscope for counting and sizing the blue PE spheres. The blue PE spheres were then rinsed into the bottles containing the (particle loaded) steel filters.

An initial density separation was necessary for HW_1 (raw Rhine River bed water) due to the high total solids content in the river water. The procedure is explained in Philipp et al. (2022). Briefly, sodium polytungstate (SPT, Roth, 8828, density = 1.9 g/cm^3) solution was used to separate commonly used plastics from mineral particles. The 20 μm stainless steel filters were placed into a 120 ml glass beaker and entirely covered with 15 ml of the SPT solution. The beaker was sonicated (TP690-A, Bioblock Scientific) for 20 s. The SPT suspension was then transferred into a 50 ml centrifuge tube. The well-mixed suspension was centrifuged at 2900 ×*g* for 45 min, and the supernatant was filtered on an Al_2O_3 membrane (Anodisc, diameter 25 mm, pore size: 0.2 μm, Whatman®).

The steel filters, still inside their bottles used during the sampling with the added blue PE spheres, from locations HW_2 to HW_6 were sonicated and the suspensions were transferred into a glass filtration column. After thoroughly rinsing the bottle walls with Milli-Q®water and ethanol, the suspensions were filtered on anodisc filters (diameter 25 mm, pore size: 0.2 μm, Whatman®). The laboratory bottles containing Milli-Q® water or ethanol were made of stiff transparent PE and the cap was made of stiff blue PE.

Replica 1 of HW_1 (HW_1_1) and HW_4_1 were disregarded from the study. This is because 50 % of the area of HW_1_1 mistakenly flushed away after removal of the filtration column while trying to detach particles sticking to the inner wall of the column. The anodisc filter HW_4_1 cracked during the transport from the filtration column towards the μFTIR instrument and it was impossible to put the filter in focus.

The very-high resolution images of the anodisc filters are uploaded on the online repository indicated in the Data Availability Section.

2.5. Microplastic identification

Microplastic particles deposited on the anodisc filter were identified using focal plane array - micro-Fourier Transform InfraRed (FPA-μFTIR) spectroscopy (Agilent Cary 670 FTIR G). Because the blue PE spheres predominantly accumulated alongside the edges of the anodisc filters (results in Section 3.1), we posed particular focus on evaluating anodisc filter areas in the inner edge and along the "rim effect". We scanned other randomly chosen areas (containing surrogate particles) in the inner filter, tentatively covering the four sectors of the filter (the sampling schema is depicted in Fig. S2). At least 50 % of each individual anodisc filter area was investigated. The evaluation of 50 % of the area of a filter amounted to about 2 working days. Such long exposure to the laboratory environment increases the chance of cross-contamination. The microFTIR instrument was operated in transmission mode and acquired two sources of information. One hyperspectral data cube of the evaluated area and one RGB image of the same area. The hyperspectral data cube was acquired using the FPA detectors capturing 64 × 64 pixels high-resolution images (pixel resolution: of 5.5 × 5.5 μm^2, spectral resolution of 4 cm^{-1}, applying 28 co-added scans, spectral range from 3900 cm^{-1} and 1250 cm^{-1}) for each single scan. The high-resolution acquisition mode is time-consuming and storage-demanding but is deemed necessary to reduce mixed spectral information within a pixel (la Cecilia et al., 2023).

We used the software Microplastics Finder (www.purency.ai) for particle identification and classification of each FPA-μFTIR evaluation (Hufnagl et al., 2019; Hufnagl et al., 2022). The software is based on random decision forests for the analysis of large FPA-μFTIR data sets of environmental samples. The model can distinguish between 22 different polymer types (Table 1) and is applicable to complex matrices. The software calculates for each identified particle two accuracy metrics: relevance (R) and similarity (S), which range between 0 (poor agreement between reference and observed spectral signatures) and 1 (high agreement). The user shall define in the software the threshold for R and S whether to retain the identified particle. The third user-defined model parameter is the minimum number of pixels (here with the size 5.5 × 5.5 μm^2) that constitute a particle (P). Yet, we carry out a sensitivity analysis on the used thresholds for R, S and P to assess their influence on the overall MPs concentration per location. For that purpose, we varied R and S from 0.0 to 0.7 with a step of 0.1 and P from 1 to 4 with a step of 1.

Table 1
Classes and acronyms of plastics targeted by the imaging software Microplastics Finder. *PA was neglected from the analyses as specified in Subsection 2.6.

Name	Acronym
Polyamide	PA*
Polypropylene	PP
Polyethylene	PE
Polyvinyl-chloride	PVC
Polyurethane	PU
Polyethylene-terephthalate	PET
Polystyrene	PS
Acryl-butadiene-styrene	ABS
Polycarbonate	PC
Poly(methyl-methacrylate)	PMMA
Cellulose-acetate	CA
Ethylene-vinyl-acetate	EVAc
Ethylene-vinyl-alcohol	EVOH
Polyacrylonitrile	PAN
Polybutylene-terephthalate	PBT
Polyether-ether-ketone	PEEK
Polyoxymethylene	POM
Polyphenylsulfone	PPSU
Polysulfone	PSU
Silicone	silicone
Polylactic-acid	PLA

The maximum and minimum Feret diameters are automatically calculated by the software Microplastics Finder. We use the maximum Feret diameter for MPs size classification. To distinguish between fibers and fragments, we use the "Aspect Ratio" defined as the ratio between "Maximum Feret Diameter" and "Minimum Feret Diameter". The MPs with an "Aspect Ratio" >3 are considered as fibers, otherwise as fragments, as in Weisser et al. (2021).

2.6. Recovery of surrogate standards and adjusted scanned area of the anodisc filter

We recorded the whole area of the anodisc filter using an optical microscope (VHX 7000, Keyence, Japan). The spiked, blue PE spheres served as surrogate standards and were located and counted manually to calculate the recovery of the blue PE spheres. The calculated recovery was assumed to be representative of any MPs in the samples, although physical properties of different materials may play a role in their recovery. The median of the recovery of blue PE spheres from the anodisc filters used in this study was 70 % (Table 2).

The total scanned area per anodisc filter was extracted from the metadata recorded by the μFTIR instrument. The total area of the anodisc filter to be possibly analyzed was calculated using the internal diameter (d) of the filtration column (d = 15.5 mm) plus a buffer to reach 17 mm given that few particles were found in the outer edge of the column. Scanned areas that did not match quality control standards (i.e., visually blurred areas particularly when blue PE spheres were not detected) were removed from the evaluated area. We also removed areas outside the outer edge of the filtration column, which were scanned by the μFTIR instrument during its rectangular scans along the edge of the filtration column. Consequently, particles in all removed areas were neglected from MPs counting.

After removal of unused areas, we scanned >50 % of the area of most anodisc filters (Table 2). Only 25 % of the area could be scanned for two anodisc filters due to the difficulty to locate portions of the filters in-focus.

Table 2
Recovery of blue PE spheres in percentage calculated as the percentage of blue PE spheres counted on the anodisc filter with respect to the number of blue PE spheres added in the sample before preparation. Adjusted scanned areas of the anodisc filters by location and replica identifier. HW_1_1 and HW_4_1 not scanned as explained in Subsection 2.4.

Location	Recovery of blue PE spheres (%)	Adjusted scanned areas [%]
HW_1_1	34	–
HW_1_2	60	75
HW_1_3	75	71
HW_1_Blank	85	31
HW_2_1	79	74
HW_2_2	85	55
HW_2_3	57	51
HW_2_Blank	76	58
HW_3_1	96	56
HW_3_2	94	44
HW_3_3	82	49
HW_3_Blank	67	45
HW_4_1	41	–
HW_4_2	43	41
HW_4_3	78	45
HW_4_Blank	40	31
HW_5_1	74	57
HW_5_2	48	43
HW_5_3	55	57
HW_5_Blank	49	64
HW_6_1	88	56
HW_6_2	57	53
HW_6_3	86	63
HW_6_Blank	29	55

2.7. Analysis of a laboratory blank

We analyzed a laboratory blank prepared by filling a glass bottle used to store the steel filter with 0.2 l Milli-Q® water. We shacked the glass bottle and then we filtered the content through a glass column on an anodisc filter (diameter 25 mm, pore size: 0.2 μm, Whatman®), as done for the environmental samples. The software identified polyamide and PMMA. Illustration of the hyperspectral signatures are provided in Section S4. The likely source of polyamide was the nylon filter within the Milli-Q® system (Schymanski et al., 2021). Indeed, the imaging software classified polyamide with good fidelity, based on visual comparison between the measured and reference hyperspectral signatures, which corresponded to the calculated minimum R of 0.59 and minimum S of 0.38. We, therefore, excluded polyamide from further analyses. PMMA in the laboratory blanks was a false positive after the visual comparison of the measured and reference hyperspectral signatures, which returned a minimum R of 0.39 and maximum S of 0.11. Thus, we included PMMA in further analyses aiming to understand whether suitable thresholds could be defined to remove false positives.

3. Results and discussions

3.1. Distribution of surrogate spheres

The approach of mapping the blue MP spheres with the optical microscope allowed for determining their distribution on the anodisc filter following filtration. The spheres often deposited alongside the inner edge of the filtration column (referred to as "rim effect") (Fig. 3). Moreover, the spheres were not evenly distributed along the edge, but they were more frequent in some sectors of the edge. This observation drove our selections of the areas to scan. More generally, the "rim effect", when present but not accounted for by means of appropriate selection of areas to scan, may have an impact on MPs number upscaling when only a portion of the filter area can be evaluated.

3.2. Variability of relevance and similarity values and definition of thresholds

The blue PE spheres were manually identified in the imaging software Microplastics Finder and programmatically: (1) we retrieved the corresponding relevance and similarity values and (2) we excluded the blue PE spheres from the overall MPs concentration. The appearance of the blue PE spheres and the corresponding hyperspectral signature is depicted in Section S5.

In this study, we followed two approaches to define the thresholds for R and S based on the type of plastics. For PE, we set the thresholds per each scanned area as the minimum R and minimum S calculated by the imaging software for the surrogate PE standards. P was kept to 1 given that the software returned 3.2 % of the surrogate standards with a size of 1 pixel, which reflected the fact that spherical particles may have the edges out of focus. As shown in Fig. 4, there is a large variability between minimum and maximum of the relevance and similarity values calculated by the model for the blue PE spheres retrieved per each replica. The variability may be due to different conditions between the

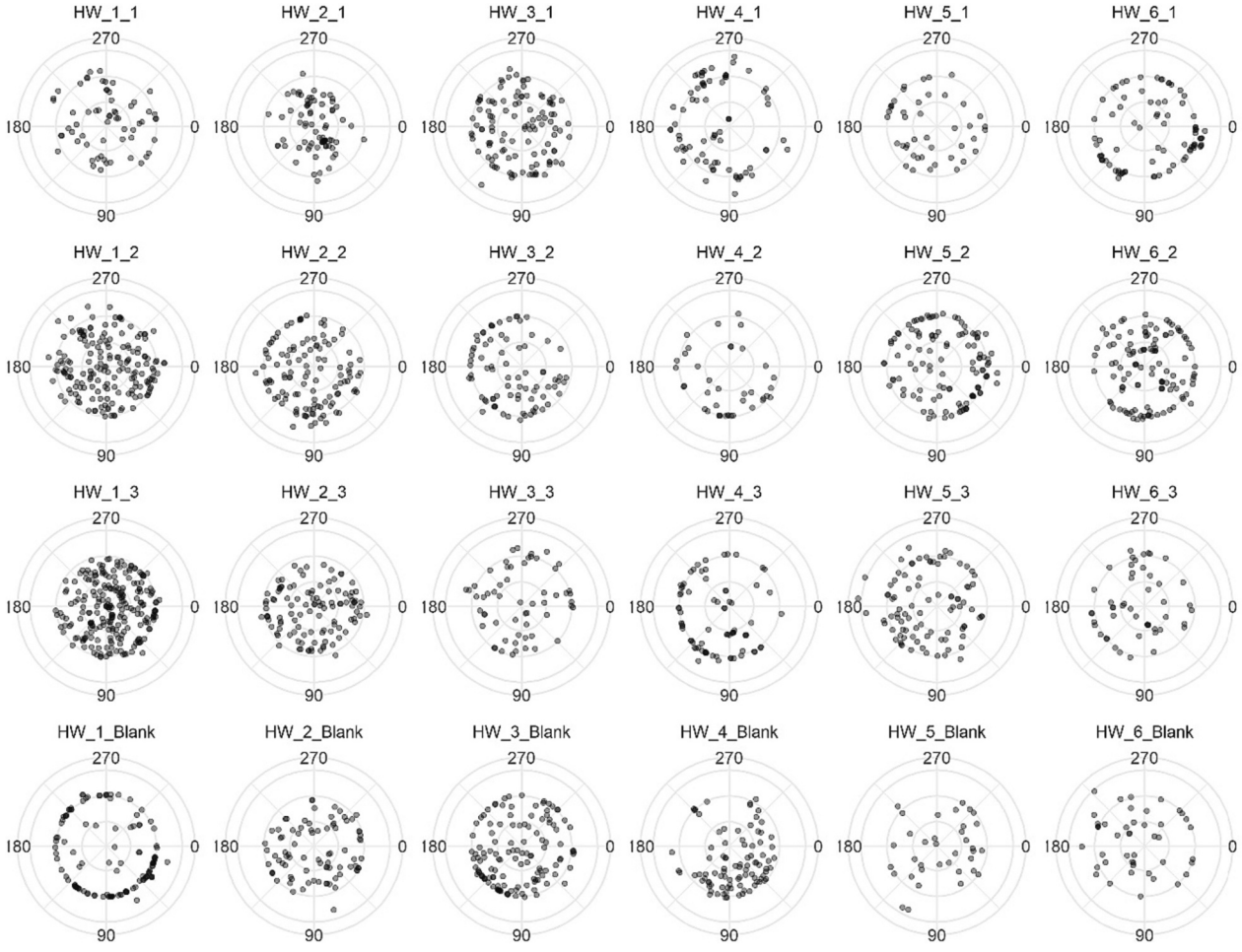

Fig. 3. Spatial distribution of blue PE spheres on the anodisc filters. The grayscale color resulted from the use of transparency for black filled points, thus isolated points appeared in light gray and overlapping points appeared in black.

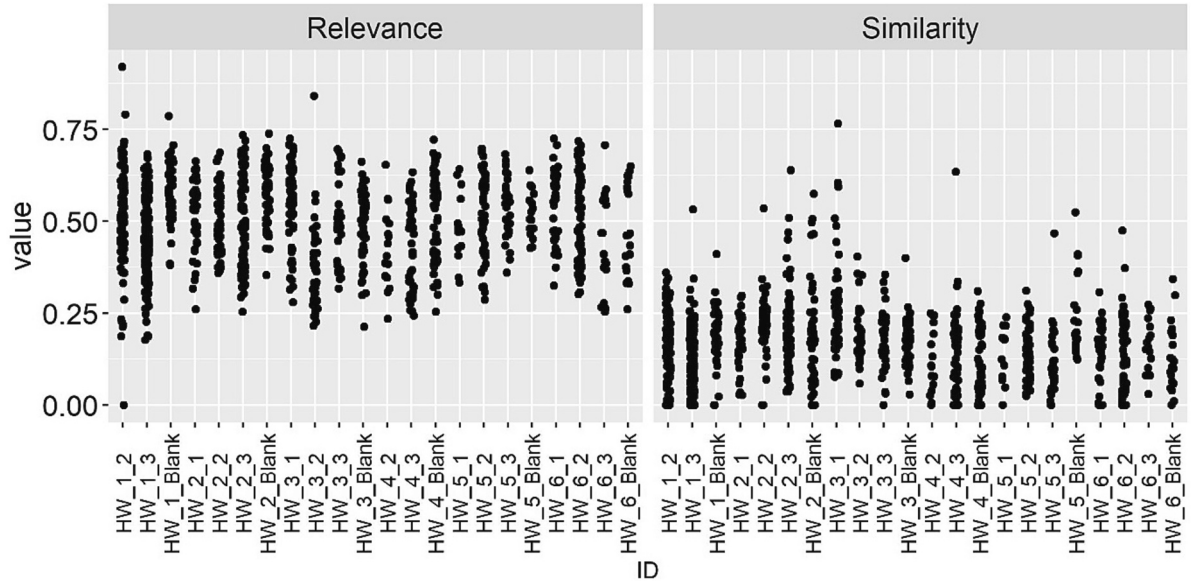

Fig. 4. Jitter plot overlaying the boxplot showing the relevance and similarity values calculated by the imaging software Microplastics Finder of the blue PE spheres retrieved from all the scanned areas.

background (clean anodisc filter) and the analyzed filter, such as: quality of the background, changes in focus, etc. Indeed, one major limitation in acquiring large continuous areas of the anodisc filters was the varying distance between the filter and the IR beam emitter, which is detrimental to the acquisition of high-quality spectra. The varying distance could be seen as a loss of focus in the RGB image. Importantly, the variability among minimum relevance and similarity values per replica did not substantially differ, which could support the approach to use one minimum reference and similarity threshold for all scanned areas. This latter was the second approach followed to define the thresholds for the other 16 types of microplastics classified in this study, for which we did not have surrogate standards. Namely, we randomly selected eleven scanned areas and we carried out a visual comparison of the measured and reference hyperspectral signature of the identified particles (Section S3). When the comparison was satisfactory, we tabulated the minimum R and S calculated by the imaging software and used them as the plastic type-specific thresholds (minimum relevance and similarity ranged between 0.1 and 0.7 as tabulated in Table S1). In the analysis of our samples, we found that the good agreement between measured and reference hyperspectral signature of PMMA occurred when the similarity was at least 0.5, used as threshold in this research as per Table S1 to effectively remove false positives (Section 2.7). This result corroborated our decision to include PMMA in our analyses.

3.3. Microplastics concentration along the water treatment system

MPs were found at all sampling locations with mean MPs concentrations across replicas decreasing from 112.0 ± 27.4 MPs/l at HW_1 (raw Rhine River bed water) to 2.0 ± 2.2 MPs/l at HW_5 (after secondary treatment, MAR and activated carbon filters), followed by a slight increase to 6.8 ± 4.0 MPs/l at HW_6 (depicted as red filled circles in Fig. 5a and reported in Table 3). The mean MPs concentration measured after the coagulation, flocculation and sedimentation step at the official sampling point for chemical studies of the raw Rhine River bed water at HW_2 was almost 20 times lower than at HW_1 with a concentration of 5.5 ± 2.2 MPs/l. The mean MPs concentration decreased by 60 times from HW_1 to the outlet of the sand filtration treatment at HW_3 with a mean concentration of 1.8 ± 0.9 MPs/l, corresponding to a removal efficiency of 98.4 %. The mean MPs concentration slightly increased after MAR to a value of 2.7 ± 0.7 MPs/l measured in the pumped groundwater at HW_4. This water is then piped to the tertiary treatment system. The mean MPs concentration slightly decreased again down to 2.0 ± 2.2 MPs/l at HW_5, before the activated carbon filters. Overall, the trend in MPs concentrations suggested that following the secondary treatment, the MPs concentration did not substantially change.

The same trend of MPs concentration from HW_1 to HW_6 was not reflected in the field blanks (Section S1). Together with the fact that our samples were exposed to the atmosphere for only a very limited time, we concluded that contamination of our water samples by MPs in the air was negligible. The use of closed filter units in this study was an appropriate choice to avoid cross-contamination of water samples by MPs in the air. Yet, we cannot exclude a cross-contamination by silicon. In fact, where we did not use silicon, the software identified four silicon particles at HW_1 (out of 3360 particles) and none at HW_4. And where we used silicon, the software identified one silicon particle at HW_3 (out of 110), 12 at HW_5 (out of 122) and none at HW_2 and HW_6.

The sensitivity analysis on the user-defined thresholds (R, S and P), whether to retain the classified MP particle revealed that the decreasing trend remained (Fig. 5b and c). However, mean MPs concentrations per location changed up to one order of magnitude depending on the used thresholds R and S. Of course, the number of MPs decreased with increasing values of R and S. Our choice to use plastic type-specific thresholds was necessary because some plastic materials have a spectral fingerprint more prone to confusion with other organic particles, and thus, they require higher thresholds In order to prevent these MPs to be erroneously accounted for in the analyses. The third model parameter P does not have a substantial impact on the measured MPs concentrations (Fig. 5c). The choice of using $P = 1$, explained in Section 3.2, corresponds to considering MPs with a minimum size of 5.5 μm, or 30.25 μm^2 (size of the pixel).

3.4. Microplastics type, length and shape along the water treatment system

Among the 17 MPs types identified, seven were found at all locations (Fig. 6). Most of the classes exceeded 1 MPs/l at HW_1 only (HW_1 in the x-axis for the 17 MPs types in Fig. 6). PE was the only class that exceeded 1 MPs/l after the tertiary treatment, achieving its second highest concentration at HW_6. This could actually be a consequence of the low similarity threshold determined using the PE surrogate standards and applied to all identified PE particles. PET, PP, PU and PVC followed a

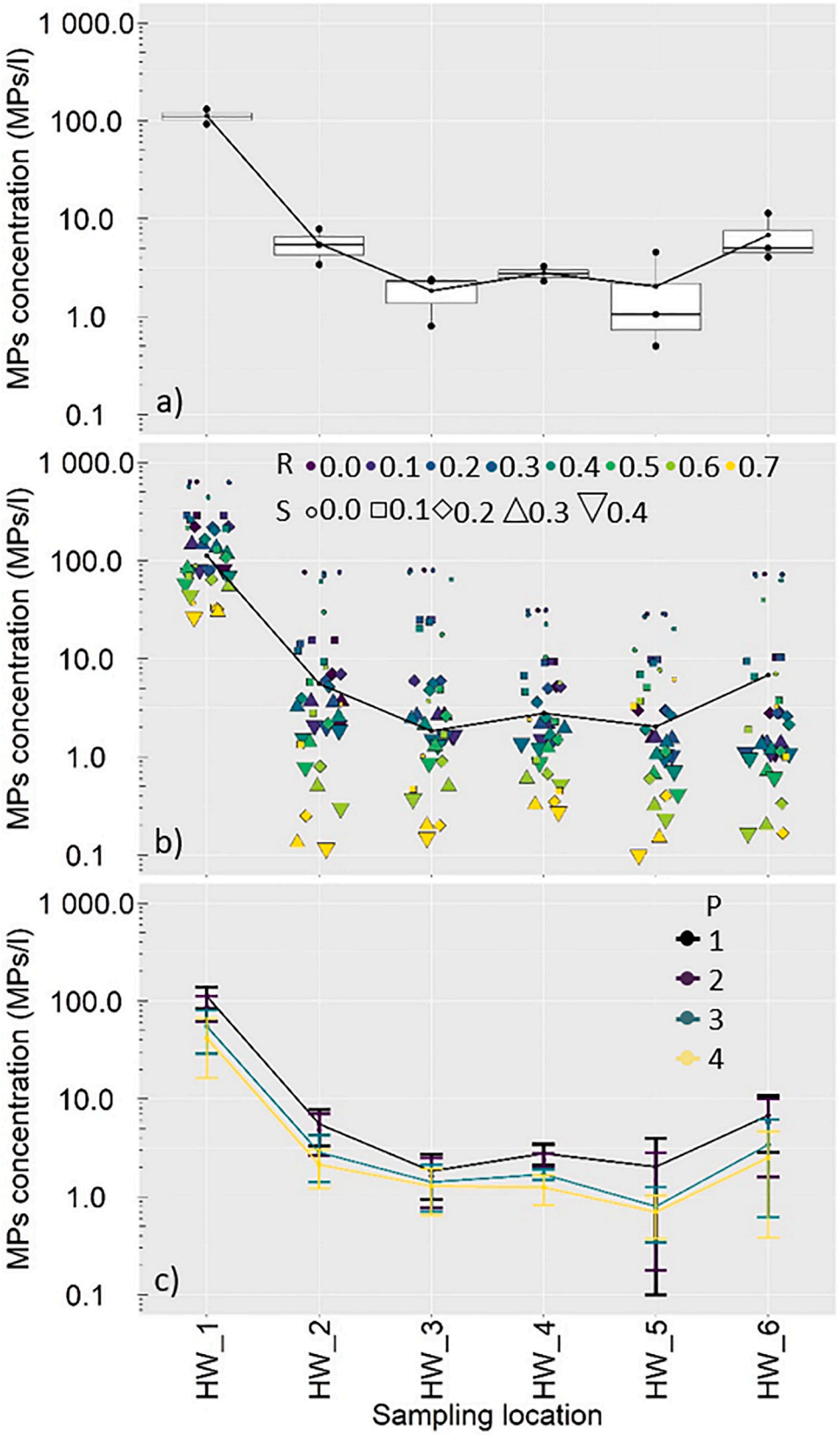

Fig. 5. MPs concentrations in log10 scale in the y-axis at the sampled locations in the x-axis. Black dotted line refers to the mean MPs concentrations among replicas per location used in this study given type-specific thresholds and $P = 1$. a) Concentration variability based on replicas. b) Concentration variability based on R and S thresholds. Different colors from purple to yellow of the symbols depict the increasing value of the threshold R from 0.0 to 0.7. Different symbols depict the increasing value of the threshold S from 0.0 to 0.4. c) Concentration variability based on the minimum number of pixels P of the particle size.

Table 3
Raw and thresholded MPs mean concentrations and standard deviations in MPs/l based on the model thresholds at the sampled locations.

Location	HW_1	HW_2	HW_3	HW_4	HW_5	HW_6
Raw (MPs/l)	635.5	76.0	79.8	31.2	28.6	72.8
Thresholded (MPs/l)	112.0 ± 27.4	5.5 ± 2.2	1.8 ± 0.9	2.7 ± 0.7	2.0 ± 2.2	6.8 ± 4.0

substantial decreasing trend in number concentration from river water to post-tertiary treatment. With the exclusion of PET, all the materials listed above can be in the composition of pipes used to transport (drinking) water. In addition, some polymers like PU can cover the inner part of steel pipes in order to reduce friction, and therefore, energy losses. Though, the detailed interpretation of the identified plastic types required a careful visual investigation of the correctness of the model classifications. While random forest is indicated for multi-label

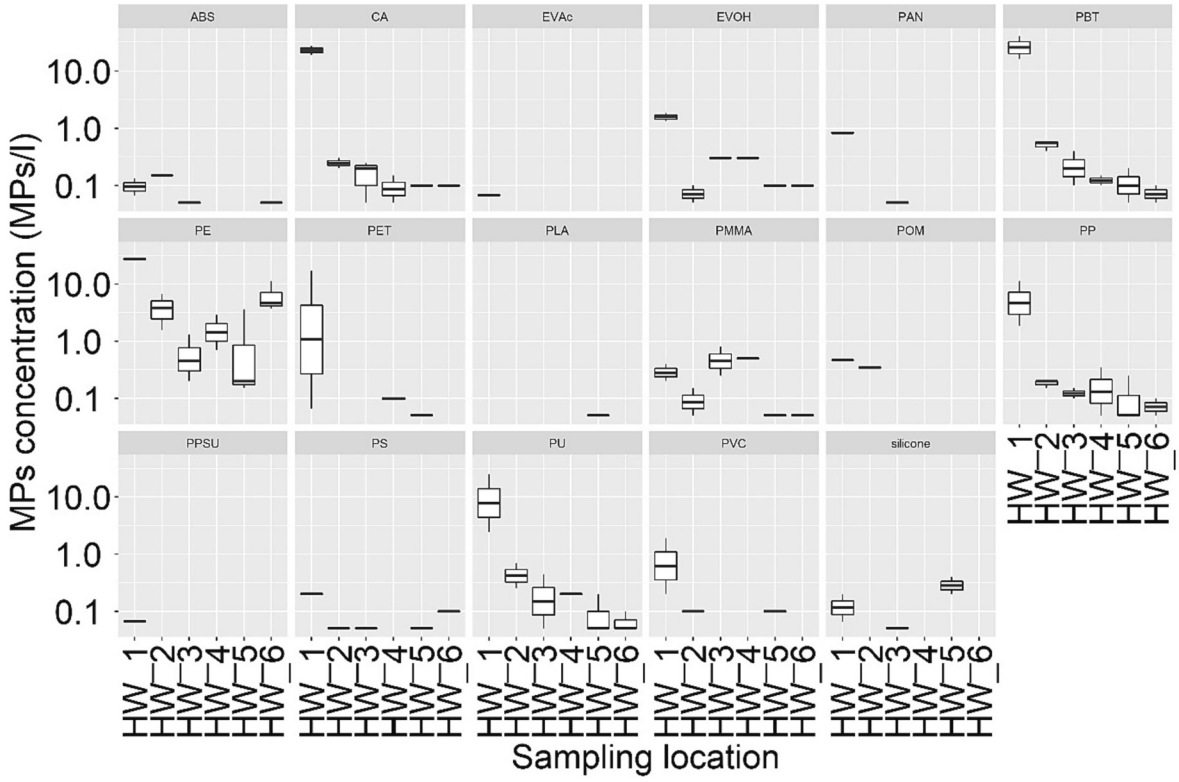

Fig. 6. Boxplots of mean MPs concentrations in log10 scale among replicas (y-axis) by sampling location (x-axis) and grouped by classes.

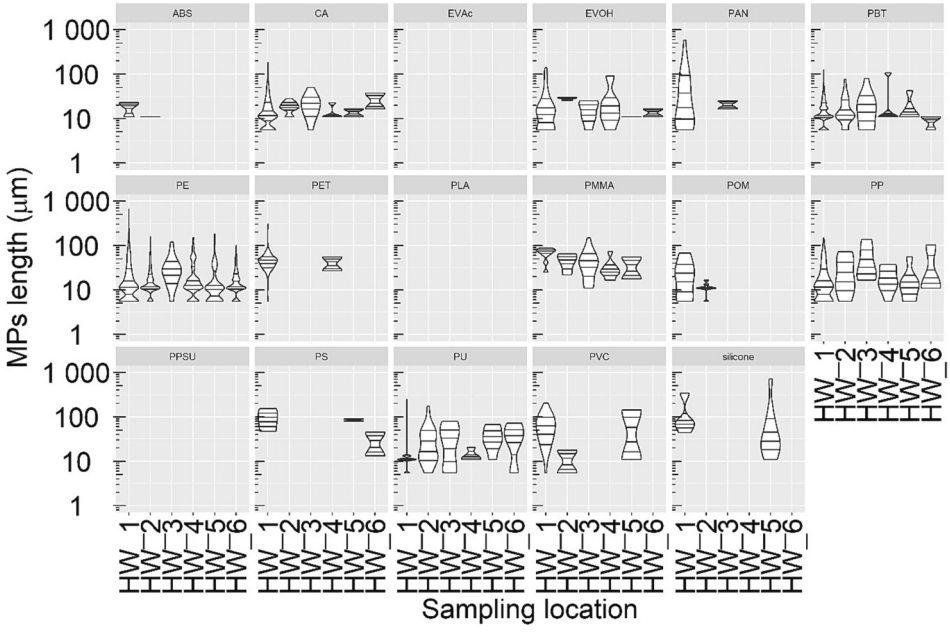

Fig. 7. Violin plots of MPs length in log10 scale (y-axis) by sampling location (x-axis) and grouped by classes. Horizontal lines indicate the quantiles 0, 0.2, 0.4, 0.6, 0.8 and 1.0. EVAc, PLA and PPSU do not appear, as compared to Fig. 6 because there were not enough data points to calculate the plotted distributions.

classification problems, dealing with a high number of classes of similar materials can be challenging due to their poor separability based on spectral signatures, which could lead to a misclassification of similar polymers (la Cecilia et al., 2023).

MPs concentration by type decreased along the MAR system (shown in Fig. 6) and MPs size did not substantially vary along the system (depicted in Fig. 7). This meant that MPs were indeed retained by the filtration systems (sand filters, MAR, activated carbon filters). Yet, mechanical abrasion with the sand grains during backwashing may cause MPs fragmentation, thus producing smaller particles (Ramirez Arenas et al., 2022). The length of the detected MPs ranged between a minimum of 5.50 μm to a maximum of 1007.75 μm, with a median of 11.00 μm (Fig. 7). Fragments prevailed over fibers (about 95 % to 5 %) at all locations according to the automatic MPs shape classification based on the threshold on the aspect ratio (Fig. 8a). Fibers were longer and more abundant at HW_1 (Fig. 8b) and this was corroborated by the visual inspection of the very-high resolution images of the anodisc filters (images available on the online repository). Nonetheless, the length of MPs particles determined using μFTIR and the MPs finder was subject to challenges also highlighted by our QA/QC method. For instance, the blue PE spheres we introduced had a nominal length ranging between 53 μm to 63 μm. However, the particle finder determined a minimum length of 5.5 μm, a median length of 55.2 μm and a maximum length of 312 μm for those blue PE spheres. With respect to the blue PE spheres, smaller lengths reflected the fact that spherical particles may have parts of them out of focus, given that μFTIR analysis scan 2D areas, and resulted smaller that they were. Similarly, fibers create another challenge because they expand in three dimensions and they are likely broken down in smaller particles when using μFTIR analysis (Philipp et al., 2022) (Fig. S5). The out of focus or non-detection of particle edges could explain the generally smaller median size too. Finally, the larger lengths were caused by particles that laid adjacent to each other, thus appearing larger than they were. To reduce this particles clustering issue, the user should manually edit each particle (Hufnagl et al., 2022).

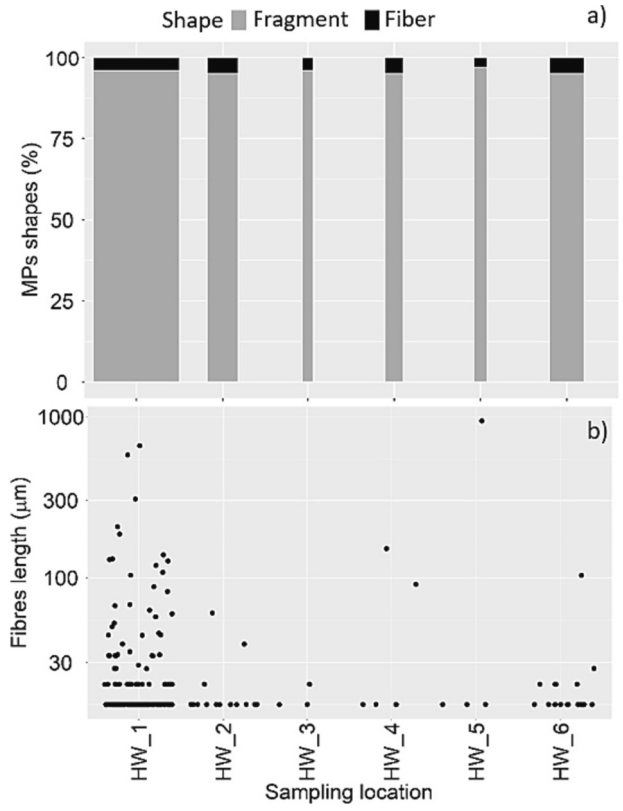

Fig. 8. a) Bar plot of the percentage of MPs as fragments or fibers grouped by location. The width of the bars is proportional to the normalized log10 of the MPs mean concentrations by location. B) Jitter plot of MPs fibers' length in log10 scale per location.

3.5. Microplastics in groundwater and monitoring challenges

In this research, we corroborate some previous literature reporting on river water contamination by MPs in Switzerland and neighboring countries (e.g., Klein et al., 2015; Thomas et al., 2015; Mennekes and Nowack, 2023). Because of river water contamination, also groundwater may potentially receive MPs transported during surface water-groundwater interactions and MAR (e.g., Viaroli et al., 2022). At our study site, however, treatment of the river water was effective to abate MPs concentrations, a result that was in line with other researches (Mintenig et al., 2019; Pulido-Reyes et al., 2022; Acarer, 2023; Islam and Islam, 2023).

Our findings demonstrate a significant reduction in MPs concentration throughout the treatment process. Starting with the water from the Rhine River bed, which had an initial concentration of 112 ± 27.4 MPs per liter, we observed a remarkable 20-fold decrease after coagulation, flocculation, and sedimentation, resulting in a concentration of 5.5 ± 2.2 MPs per liter. Further treatment through the sand-filtration system led to a 3-fold reduction, resulting in an even lower concentration of 1.8 ± 0.9 MPs per liter. This cumulative process achieved an overall removal efficiency of 98.4 %. Even as the water passed through a Quaternary gravel aquifer during MAR, MP concentrations remained consistently low at 2.7 ± 0.7 MPs per liter. Notably, the introduction of activated carbon filters did not significantly contribute to further decreasing MPs concentrations. Throughout these stages, the majority of MPs present were in the form of fragments, comprising approximately 95 % of the total, while fibers accounted for the remaining 5 %. Overall, it seems that MAR through soils characterized by small pore sizes can contribute to further decreasing MPs concentrations (Re, 2019). Very large pores are likely in the first meter of soil column due to bioturbation and the gravel layer (see Section 2.1), but given a soil profile of tens of meters at our MAR site with natural soil, we can expect that smaller pores can trap and attenuate MPs passing the secondary treatment, which shows already a significant reduction of MPs.

Current monitoring and measuring approaches, from sampling to quantification, are time-consuming and subject to uncertainties and constraints. We are limited to MPs larger than 20 μm, and therefore, we cannot adequately study the transport behaviour of smaller MPs in the aquifer. Still, some first studies on the topic indicate that the transport of MPs smaller than 20 μm in the subsurface is potentially taking place (Panno et al., 2019, Viaroli et al., 2022; Goeppert and Goldscheider, 2021, Moeck et al., 2023). While Goeppert and Goldscheider (2021) show that transport of MPs in alluvial aquifers over larger distances is possible, quantitative studies regarding the direct input of MPs through groundwater management practices are still lacking.

Apart from the challenge deriving from the analytical resolution, very frequently for our samples it was necessary to adjust the focus on the anodisc filter to be measured, thus deviating from the calibration step acquired using another background anodisc filter. These changes in focus can have an impact on the quality of the acquired hyperspectral map. Moreover, methods to prevent the "out-of-focus" as well as the "rim effect" (please see Fig. 3) issues are urged to achieve a high-quality and complete hyperspectral map of the anodisc filter. In this study, we observed that the focus between the center of the filter and the edges of the filtration area varied, also due to the bending of the filter surface. The uneven distribution of the surrogate standards, with an accumulation at the edges of the filtration column, brought about challenges with upscaling approaches. Given the large scanned areas (> 50 %) and the focus on scanning area along comprising the "rim effect", we assume that these were minor issues in our study but systematic investigations are required.

4. Conclusions

Managed Aquifer Recharge (MAR) is essential to increase the volume of groundwater available for drinking water production, but may pose a threat to groundwater quality by introducing synthetic contaminants from surface water, such as MPs. In this study, we investigated the fate of MPs at various stages at a MAR-water supply system in Switzerland, from the affluent river water to the effluent drinking water. Although, MPs were found at all sampling locations, our findings revealed a remarkable 60-fold decrease in MPs concentration from the Rhine River bed water (112.0 ± 27.4 MPs/l) to after secondary treatment (flocculation, sedimentation and sand filtration) (1.8 ± 0.9 MPs/l), corresponding to a removal efficiency of 98.4 %. Subsequently, the MPs concentrations did not change substantially following MAR into a Quaternary gravel aquifer and the activated carbon filters. We excluded that MPs concentration decreased simply due to particles increasing in size (possibly following coagulation or agglomeration), and therefore, MPs were effectively retained by the treatment systems.

Moreover, we found a sensitivity of the model classification output to the thresholds R and S. Changing R and S values changed up to one order of magnitude the mean MPs concentrations per location, but they did not impact the general decreasing trend along the treatment system. The sensitivity of MPs concentrations to the parameters of the classification models is rarely reported, but it shall be for proper comparisons among field studies. Finally, the quantifications of MPs is often subject to upscaling estimates. Here, we observed an uneven distribution of surrogate MPs on the filter, with the surrogate standards increasing in numbers from the center to the edge and being unevenly spread across sectors of the filters. We considered these patterns by carefully selecting the filter areas to scan. While uncertainties exist in MPs monitoring, this study provided further evidence on the effectiveness of the treatment systems in removing MPs larger than 20 μm, which shall be designed to protect groundwater resources.

Authors contributions

CM, DLC and MS conceptualized the study. CM and DLC carried out the field sampling. DLC carried out the laboratory analyses. MP provided support with laboratory analyses. DLC performed the data analysis. CM provided feedbacks on data analysis. All authors contributed to data interpretation. DLC drafted the first version of the manuscript. CM and RK provided feedbacks in the initial stages of the manuscript. All authors contributed to review the manuscript until its submission. MS acquired the funding for this research.

Declaration of competing interest

The authors declare that they have no known competing financial interests or personal relationships that could have appeared to influence the work reported in this paper.

Data availability

Raw files have a size of about 2 TB, and can be requested to Reto Britt (reto.britt@eawag.ch) up to 10 years since the publication of the manuscript upon reasonable request. The very-high resolution images of the anodisc filters, the data produced with the imaging software Microplastics Finder (www.purency.ai) and scripts used to generate the plots will be available through the Eawag data repository ERIC at the link "https://doi.org/10.25678/0009E6" to ensure that data and methods are FAIR: Findable, Accessible, Interoperable and Reproducible.

Acknowledgements

We thank our colleague at Eawag Reto Britt for the realization of the sampling device, the acquisition of samples during the sampling campaign and assistance in the particle laboratory for sample analysis. We acknowledge our colleague Marie-Sophie Maier for assisting in the sample acquisition at location 1. We deeply thank the drinking water production plant for allowing us to carry out the study in their facility and the useful discussions. This research received funding from the European Union's Horizon 2020 Research and Innovation programme under grant agreement No. 776866 for the research project RECONECT (Regenerating ECOsystems with Nature-based solutions for hydro-meteorological risk rEduCTion). We thank the two anonymous reviewers who with their comments contributed to enhance the quality of the manuscript.

Appendix A. Supplementary data

Supplementary data to this article can be found online at https://doi.org/10.1016/j.scitotenv.2023.168378.

References

Acarer, S., 2023. Abundance and characteristics of microplastics in drinking water treatment plants, distribution systems, water from refill kiosks, tap waters and bottled waters. Sci. Total Environ. 884, 163866 https://doi.org/10.1016/j.scitotenv.2023.163866.

Arthur, C., Baker, J., Bamford, H., 2009. Proceedings of the International Research Workshop on the Occurrence, Effects, and Fate of Microplastic Marine Debris. *NOAA Technical Memorandum* NOS-OR&R-30.

Belkhiri, A.H., Carre, F., Quiot, F., 2022. State of knowledge and future research needs on microplastics in groundwater. J. Water Health 20 (10), 1479–1496. https://doi.org/10.2166/wh.2022.048.

Boos, J.P., Gilfedder, B.S., Frei, S., 2021. Tracking microplastics across the streambed interface: using laser-induced-fluorescence to quantitatively analyze microplastic transport in an experimental flume. Water Resour. Res. 57, e2021WR031064.

la Cecilia, D., Tom, M., Stamm, C., Odermatt, D., 2023. Pixel-based mapping of open field and protected agriculture using constrained Sentinel-2 data. ISPRS Open Journal of Photogrammetry and Remote Sensing 8. https://doi.org/10.1016/j.ophoto.2023.100033.

Crossman, J., Hurley, R.R., Futter, M., Nizzetto, L., 2020. Transfer and transport of microplastics from biosolids to agricultural soils and the wider environment. Sci. Total Environ. 724, 138334 https://doi.org/10.1016/j.scitotenv.2020.138334.

Epting, J., Vinnå, L.R., Piccolroaz, S., Affolter, A., Scheidler, S., 2022. Impacts of climate change on Swiss alluvial aquifers – a quantitative forecast focused on natural and artificial groundwater recharge by surface water infiltration. Journal of Hydrology X 17, 100140. https://doi.org/10.1016/j.hydroa.2022.100140.

Frias, J.P.G.L., Nash, R., 2019. Microplastics: finding a consensus on the definition. Mar. Pollut. Bull. 128, 145–147. https://doi.org/10.1016/j.marpolbul.2018.11.022.

Goeppert, N., Goldscheider, N., 2021. Experimental field evidence for transport of microplastic tracers over large distances in an alluvial aquifer. J. Hazard. Mater. 408, 124844.

Hale, R.C., Seeley, M.E., La Guardia, M.J., Mai, L., Zeng, E.Y., 2020. A global perspective on microplastics. J. Geophys. Res. Oceans 125 (1). https://doi.org/10.1029/2018jc014719.

Hartmann, N.B., Hüffer, T., Thompson, R.C., Hassellöv, M., Verschoor, A., Daugaard, A.E., Rist, S., Karlsson, T., Brennholt, N., Cole, M., Herrling, M.P., Hess, M.C., Ivleva, N.P., Lusher, A.L., Wagner, M., 2019. Are we speaking the same language? Recommendations for aDefinition and categorization framework for plastic debris. Environ. Sci. Technol. 53, 1039–1047. https://doi.org/10.1021/acs.est.8b05297.

Hufnagl, B., Steiner, D., Renner, E., Löder, M.G.J., Laforsch, C., Lohninger, H., 2019. A methodology for the fast identification and monitoring of microplastics in environmental samples using random decision forest classifiers. Anal. Methods 11 (17), 2277–2285. https://doi.org/10.1039/c9ay00252a.

Hufnagl, B., Stibi, M., Martirosyan, H., Wilczek, U., Moller, J.N., Loder, M.G.J., Lohninger, H., 2022. Computer-assisted analysis of microplastics in environmental samples based on muFTIR imaging in combination with machine learning. Environ. Sci. Technol. Lett. 9 (1), 90–95. https://doi.org/10.1021/acs.estlett.1c00851.

Islam, M.S., Islam, Z.A.H.M.S., Islam Jamal, M., Montaz, N., Beauty, S.A., 2023. Removal efficiencies of microplastics of the three largest drinking water treatment plants in Bangladesh. Sci Tot Env 895, 165155. https://doi.org/10.1016/j.scitotenv.2023.165155.

Johnson, A.C., Ball, H., Cross, R., Horton, A.A., Jurgens, M.D., Read, D.S., Svendsen, C., 2020. Identification and quantification of microplastics in potable water and their sources within water treatment works in England and Wales. Environ. Sci. Technol. 54 (19), 12326–12334. https://doi.org/10.1021/acs.est.0c03211.

Kernchen, S., Loder, M.G.J., Fischer, F., Fischer, D., Moses, S.R., Georgi, C., Laforsch, C., 2022. Airborne microplastic concentrations and deposition across the Weser River catchment. Sci. Total Environ. 818, 151812 https://doi.org/10.1016/j.scitotenv.2021.151812.

Klein, S., Worch, E., Knepper, T.P., 2015. Occurrence and spatial distribution of microplastics in river shore sediments of the Rhine-Main area in Germany. Environ Sci Tec 49, 6070–6076. https://doi.org/10.1021/acs.est.5b00492.

Koelmans, A.A., Mohamed Nor, N.H., Hermsen, E., Kooi, M., Mintenig, S.M., De France, J., 2019. Microplastics in freshwaters and drinking water: critical review and assessment of data quality. Water Res. 155, 410–422. https://doi.org/10.1016/j.watres.2019.02.054.

Mennekes, D., Nowack, B., 2023. Predicting microplastic masses in river networks with high spatial resolution at country level. Nature Water 1-11. https://doi.org/10.1038/s44221-023-00090-9.

Mintenig, S.M., Löder, M.G.J., Primpke, S., Gerdts, G., 2019. Low numbers of microplastics detected in drinking water from ground water sources. Sci. Total Environ. 648, 631–635. https://doi.org/10.1016/j.scitotenv.2018.08.178.

Moeck, C., Radny, D., Borer, P., Rothardt, J., Auckenthaler, A., Berg, M., Schirmer, M., 2016. Multicomponent statistical analysis to identify flow and transport processes in a highly-complex environment. J. Hydrol. 542, 437–449.

Moeck, C., Radny, D., Popp, A., Brennwald, M., Stoll, S., Auckenthaler, A., Schirmer, M., 2017a. Characterization of a managed aquifer recharge system using multiple tracers. Sci. Total Environ. 609, 701–714. https://doi.org/10.1016/j.scitotenv.2017.07.211.

Moeck, C., Radny, D., Auckenthaler, A., Berg, M., Hollender, J., Schirmer, M., 2017b. Estimating the spatial distribution of artificial groundwater recharge using multiple tracers. Isotopes Environ. Health Stud. 53, 484–499. https://doi.org/10.1080/10256016.2017.1334651.

Moeck, C., Davies, G., Krause, S., et al., 2023. Microplastics and nanoplastics in agriculture—A potential source of soil and groundwater contamination? Grundwasser - Zeitschrift der Fachsektion Hydrogeologie 28, 23–35. https://doi.org/10.1007/s00767-022-00533-2.

Moses, S.R., Roscher, L., Primpke, S., et al., 2023. Comparison of two rapid automated analysis tools for large FTIR microplastic datasets. Anal. Bioanal. Chem. https://doi.org/10.1007/s00216-023-04630-w.

Panno, S.V., Kelly, W.R., Scott, J., Zheng, W., McNeish, R.E., Holm, N., Hoellein, T.J., Baranski, E.L., 2019. Microplastic contamination in karst groundwater systems. Groundwater 57, 189–196.

Philipp, M., Bucheli, T.D., Kaegi, R., 2022. The use of surrogate standards as a QA/QC tool for routine analysis of microplastics in sewage sludge. Sci. Total Environ. 835, 155485 https://doi.org/10.1016/j.scitotenv.2022.155485.

Pivokonsky, M., Cermakova, L., Novotna, K., Peer, P., Cajthaml, T., Janda, V., 2018. Occurrence of microplastics in raw and treated drinking water. Sci. Total Environ. 643, 1644–1651. https://doi.org/10.1016/j.scitotenv.2018.08.102.

PlasticEurope, 2022. Plastics – the Facts 2022, 81.

Popp, A.L., Scheidegger, A., Moeck, C., Brennwald, M.S., Kipfer, R., 2019. Integrating Bayesian groundwater mixing modeling with on-site helium analysis to identify unknown water sources. Water Resour. Res. 55 (12), 10602–10615. https://doi.org/10.1029/2019WR025677.

Pulido-Reyes, G., Magherini, L., Bianco, C., Sethi, R., von Gunten, U., Kaegi, R., Mitrano, D.M., 2022. Nanoplastics removal during drinking water treatment: laboratory- and pilot-scale experiments and modeling. J. Hazard. Mater. 436, 129011 https://doi.org/10.1016/j.jhazmat.2022.129011.

Ramirez Arenas, L., Ramseier Gentile, S., Zimmermann, S., Stoll, S., 2022. Fate and removal efficiency of polystyrene nanoplastics in a pilot drinking water treatment plant. Sci. Total Environ. 813, 152623 https://doi.org/10.1016/j.scitotenv.2021.152623.

Re, V., 2019. Shedding light on the invisible: addressing the potential for groundwater contamination by plastic microfibers. Hydrgeol. J. 27 (7), 2719–2727. https://doi.org/10.1007/s10040-019-01998-x.

Reed, C., 2015. Dawn of the plasticene age. New Scientist 225 (3006), 28–32. https://doi.org/10.1016/s0262-4079(15)60215-9.

Rosario-Ortiz, F., Rose, J., Speight, V., von Gunten, U., Schnoor, J., 2016. How do you like your tap water? Safe drinking water may not need to contain a residual disinfectant. Science 351, 912–914. https://doi.org/10.1126/science.aaf0953.

Ross, M.S., Loutan, A., Groeneveld, T., Molenaar, D., Kroetch, K., Bujaczek, T., Ruecker, N.J., 2023. Estimated discharge of microplastics via urban stormwater during individual rain events. Front. Environ. Sci. 11 https://doi.org/10.3389/fenvs.2023.1090267.

Schymanski, D., Ossmann, B.E., Benismail, N., Boukerma, K., Dallmann, G., von der Esch, E., Ivleva, N.P., 2021. Analysis of microplastics in drinking water and other clean water samples with micro-Raman and micro-infrared spectroscopy: minimum requirements and best practice guidelines. Anal. Bioanal. Chem. 413 (24), 5969–5994. https://doi.org/10.1007/s00216-021-03498-y.

Strand, J., Feld, L., Murphy, F., Mackevica, A., Hartmann, N.B., 2018. Analysis of microplastic particles in Danish drinking water. Aarhus University, DCE – Danish Centre for Environment and Energy., Scientific Report No. 291, 34.

Thomas, M., Hauk, A., Walter, U., Burkhardt-Holm, P., 2015. Microplastics profile along the Rhine River. Sci. Rep. 5, 17988. https://doi.org/10.1038/srep17988.

Tian, W., Song, P., Zhang, H., Duan, X., Wei, Y., Wang, H., Wang, S., 2023. Microplastic materials in the environment: problem and strategical solutions. Prog. Mater. Sci. 132 https://doi.org/10.1016/j.pmatsci.2022.101035.

Treilles, R., Gasperi, J., Gallard, A., Saad, M., Dris, R., Partibane, C., Tassin, B., 2021. Microplastics and microfibers in urban runoff from a suburban catchment of greater Paris. Environ. Pollut. 287, 117352 https://doi.org/10.1016/j.envpol.2021.117352.

Velasco, A.N., Gentile, S.R., Zimmermann, S., Le Coustumer, P., Stoll, S., 2023. Contamination and removal efficiency of microplastics and synthetic fibres in a conventional drinking water treatment plant in Geneva, Switzerland. Sci. Total Environ. 880, 163270 https://doi.org/10.1016/j.scitotenv.2023.163270.

Viaroli, S., Lancia, M., Re, V., 2022. Microplastics Contamination of Groundwater: Current Evidence and Future Perspectives. Sci. Total. Environ, A review. https://doi.org/10.1016/j.scitotenv.2022.153851.

Wada, Y., 2016. Modeling groundwater depletion at regional and global scales: present state and future prospects. Surv. Geophys. 37, 419–451. https://doi.org/10.1007/s10712-015-9347-x.

Waldschläger, K., Lechthaler, S., Stauch, G., Schüttrumpf, H., 2020. The way of microplastic through the environment – application of the source-pathway-receptor model (review). Sci. Total Environ. 713 https://doi.org/10.1016/j.scitotenv.2020.136584.

Wang, Z., Lin, T., Chen, W., 2020. Occurrence and removal of microplastics in an advanced drinking water treatment plant (ADWTP). Sci. Total Environ. 700, 134520 https://doi.org/10.1016/j.scitotenv.2019.134520.

Weisser, J., Beer, I., Hufnagl, B., Hofmann, T., Lohninger, H., Ivleva, N.P., Glas, K., 2021. From the well to the bottle: identifying sources of microplastics in mineral water. Water 13, 841. https://doi.org/10.3390/w13060841.

Xu, Y., Ou, Q., Wang, X., Hou, F., Li, P., van der Hoek, J.P., Liu, G., 2023. Assessing the mass concentration of microplastics and Nanoplastics in wastewater treatment plants by pyrolysis gas chromatography-mass spectrometry. Environ. Sci. Technol. 57 (8), 3114–3123. https://doi.org/10.1021/acs.est.2c07810.